FATIGUE STUDIES OF SINGLE CRYSTAL BERYLLIUM*

by

J. F. Breedis, A. Lawley and J. A. Zeiger

The Franklin Institute Laboratories, Philadelphia, Pennsylvania

*This research was supported by the National Aeronautics and Space Administration under contract NASr-145.

ABSTRACT

32894

Transmission electron microscope studies have been made of the dislocation arrangements in zone-refined Pechiney beryllium oriented for basal or prism slip following fatigue at room temperature. Fatigue modes include (i) reverse bending at 1800 cpm (ii) low frequency ($\sim$ 2 cpm) uniaxial tension or compression cycling. The surface slip structure in bend fatigue was examined optically and also by using high resolution silicon monoxide replicas.

Crystals oriented for basal slip in bend fatigue do not develop a persistent slip structure at the surface. However, in the case of prism slip, additional deformation takes place by cross-slip on the basal plane, and persistent slip bands are observed below the surface. These bands consist of intrusions and extrusions. After reverse bending the surface layers show a high density of small circular prismatic loops $\sim$ 250Å, and bundles of dislocations elongated in the $[0\bar{1}10]$ direction. Axial fatigue gives rise to a relatively uniform dislocation substructure of edge and screw components and prismatic dislocation loops. After prolonged examination in the electron microscope, bend fatigue crystals recover by a combination of prismatic glide and climb of prismatic loops. In order to promote recovery following axial fatigue, it is necessary to heat the foil to a temperature in the range 100-200°C. The dislocation loops formed by fatigue damage or by recovery have a Burgers vector out of the plane of the loop.

I. Introduction

The deformation behavior of beryllium under conditions of cyclic loading, both at high and low frequencies, has been largely neglected. Our current knowledge of fatigue in this material is restricted to a small number of conventional S-N plots for commercial grades. Wallace and Wallace (1) report an endurance limit ~ 31,000 psi for polycrystalline hot pressed and warm extruded material in axial tension-compression. More recently, Klein et al (2) have obtained improved bend fatigue strength (endurance limit ~ 40,000 psi) in QMV beryllium sheet which was produced by vacuum hot working.

Several studies have been aimed at an understanding of plastic flow in beryllium through direct observation of glide dislocation configurations. These include the examination of both polycrystalline (3.4) and single crystal (3,5) beryllium covering a wide range of purities. No studies of this nature have been reported involving cyclic loading; in fact, only a limited number of electron microscope observations have been made on fatigued hexagonal close-packed metals, and these refer to magnesium (6) and zinc (7). In these instances, the deformation structure is similar to that of the face-centered cubic metals copper and nickel (8) following fatigue. Dense bundles of elongated edge dipoles are observed in the active slip plane with a direction of elongation $\langle 10\bar{1}0 \rangle$ normal to the Burgers vector. There is a relative absence of dislocations having a large screw component, and the dislocation density between bundles is extremely low.

In the present investigation high purity single crystals of

beryllium have been plastically deformed under conditions of bending and axial fatigue. The dislocation configurations in crystals oriented for basal and prism glide are compared with those reported by Damiano and Herman (5) for material of comparable purity deformed in unidirectional tension. In addition, the dislocation distribution has been correlated with surface slip line observations.

2. Experimental Procedure

a. Specimen Preparation: Single crystals of beryllium were grown from 0.5" dia. PECHINEY secondary refined vacuum cast and extruded stock using the floating zone melting technique developed by Spangler et al (9). Crystals received three zone passes, and specific orientations were obtained by seeding. All the necessary shaping operations were performed by low energy, spark discharge machining. Prior to fatigue testing, specimens were given a final electropolish in a solution of 50 parts ethylene glycol, 5 parts concentrated nitric acid, 1 part concentrated sulphuric acid, and 1 part concentrated hydrochloric acid, using a potential of 15 volts. The geometry and dimensions of the specimens are illustrated in FIGURE 1. For compression fatigue, the specimens were cylinders of height 0.58" and diameter 0.30". The crystallographic code for the planes A and B, and the angle Φ is given in TABLE 1. The shape of the bend fatigue specimen is such that the bending stress is constant along the length of the crystal.

b. Fatigue Testing: Bend fatigue tests were made in a Sonntag SF-2-U machine at 1800 cpm. Crystals oriented for basal slip were subjected to reverse bending about a mean zero stress so that the upper and lower surfaces (FIGURE 1a) were alternately in tension and compression. For the prism slip

orientation, compressive stresses lead to twinning on $\{10\bar{1}2\}$ planes. Accordingly, the crystals were fatigued in simple bending whereby the upper surface is subjected to only cyclic tensile stress, and the lower surface to only cyclic compressive stress. For the two crystal orientations studied, the load was increased to a level at which the resolved surface stress on the prism or basal slip systems was approximately three times that required for plastic flow. These critical resolved shear stresses, as determined previously in tension on crystals of identical orientation, are $\sim$ 860 psi and $\sim$ 7900 psi for basal and prism slip respectively. At these stresses, the basal and prism crystals were subjected to 2×10^6, and 5×10^6 cycles, respectively, without fracture.

Low frequency ($\sim$ 2 cpm) tensile and compressive axial fatigue tests were made in a straining jig which is located between the fixed and moving crosshead of a standard Instron machine. Details of the complete assembly are described elsewhere (10). It should be emphasized that the jig was designed for studies of the microplastic strain region in materials ($\Delta\ell / \ell \simeq 10^{-6}$), so that extremely accurate alignment of the specimen axis and stress axis is possible. The compression and tension fatigue damage was induced under conditions of constant strain amplitude at the macroscopic yield stress. In both compression and tension fatigue, the resolved glide strain on the basal and prism slip systems, respectively was 0.0015 per cycle for a total of 45 cycles.

c. Electron Microscopy: Initially, the fatigued crystals were examined under the light microscope for slip lines. High resolution replicas were then prepared from the surface using the method of Grube and Rouze (11). A water soluble agent, Victawet 35B, is first evaporated onto the beryllium

surface followed by evaporation of SiO. In this way the replicas can be removed from the surface by immersion in distilled water. Replicas were shadowed with tungsten oxide prior to examination in the electron microscope.

Thin foils suitable for transmission electron microscopy were prepared from slices of selected orientation using the jet polishing technique followed by a final electropolish in the ethylene glycol-acid solution. The slices were cut from the bulk crystal using the low energy, spark discharge method. The foils were examined in transmission in a Philips 100B electron microscope operating at either 80KV or 100KV. Selected area electron diffraction was used to index directions in the plane of the foil; as a further check on orientation, a standard back reflection x-ray Laue photograph was taken with the foil in the microscope holder, prior to examination in the microscope. Burgers vectors were studied using specific diffraction contrast conditions.

3. Electron Microscope Observations

In presenting the experimental observations, it is convenient to consider: (a) the basal slip condition in bend and axial fatigue, and (b) the prism slip condition in bend and axial fatigue.

a. Crystals Oriented for Basal Slip: Consideration is given first to the crystals of basal slip orientation fatigued in the reverse bend mode. A representative light micrograph, and electron micrograph of the replicated surface are illustrated in FIGURE 2. Geometrically, the surface of observation in both the micrographs corresponds to the point of emergence of edge dislocations having a Burgers vector $\frac{1}{3}[\bar{2}110]$ (refer to FIGURE 1). Thus, the slip traces are parallel to $[01\bar{1}0]$ which is the line of intersection

of the basal plane and the surface of observation. Slip has occurred over the entire gauge section, and in the central region away from either grip is on a relatively fine scale. In regions adjacent to the grips, deeper slip steps are frequently observed, indicating that stress concentrations exist in these regions. From a detailed examination of the surface replicas, no activity on other systems such as those involving the prism plane was observed. After 2×10^6 cycles at a resolved stress of 2,700 psi on the $(0001)\ \frac{1}{3}\ [\bar{2}110]$ system, the resolved stress was increased to 3,000 psi causing fracture at the fixed grip after a further 2×10^4 cycles. No persistent slip structure was observed by replication after electropolishing of this surface to a depth of approximately 1μ.

Preparation of transmission foils by the jet polishing technique allows for observation at varying depths below the surface of maximum bending stress. It was determined in this way that the bend fatigue damage is confined to the surface layers within approximately 30 to 50μ of the surface. Foils prepared from the bend fatigue specimen contained a high density of dislocations ($\sim 10^{10}$ cm.cm^{-3}); a dislocation substructure representative of the entire deformed crystal could not be defined since distinct differences in configuration were observed from region to region, and also from adjacent areas within the same foil. The dislocation configurations in FIGURE 3 summarize these variations. In each of the micrographs the plane of the foil is very nearly $(\bar{2}113)$ with the basal plane at an inclination of 43° from the foil plane. By the use of selected diffraction contrast conditions, it was established that many of the dislocations visible in FIGURE 3a do not belong to the preferred $(0001)\ \frac{1}{3}\ [\bar{2}110]$ slip system. Specifically, strong contrast

conditions exist using the $[01\bar{1}0]$ reflection, a reflection for which (g.b)s is zero when the Burgers vector is $\frac{1}{3}[\bar{2}110]$. This implies the presence of dislocations on the basal plane having a Burgers vector of either $\frac{1}{3}[1\bar{2}10]$ or $\frac{1}{3}[11\bar{2}0]$.

The slip bands observed in the surface replicas are also recognizable as the planar dislocation arrays in FIGURE 3a. The foil thickness in this case, as determined from projected dislocation lengths, varied from $\sim$ 1000 Å in the center of the micrograph to $\sim$ 4000 Å in the upper left-hand corner. A resolvable slip band structure is evident in FIGURE 3b and in addition, dislocation loops are present which are not necessarily confined to bands. In projection, the loops are nearly circular or highly elongated along the $[01\bar{1}0]$ direction, the shape of the former being compatible with their lying on the inclined basal plane. For an average loop diameter of 250 Å, the loop density approaches 10^{15} cm^{-3}. Although the general features observed in FIGURE 3c resemble closely those of FIGURE 3b it is evident that few glide dislocations are present in the former. It is possible in this instance, that some form of recovery has taken place, whereby the glide dislocations are converted into prismatic dislocation loops. Recovery processes actually observed in highly deformed, high-purity beryllium are considered in detail in a subsequent section.

The dislocation networks depicted in FIGURE 3d constitute a fourth type of dislocation substructure. The networks form extensive boundaries and presumably lie on the basal plane. In agreement with earlier observations (3,5), the nodes within the networks are not visibly extended. This is consistent with the supposed relatively high stacking fault energy of beryllium.

The axial compression fatigue specimens oriented for basal slip were given a total glide strain of 0.07. Thin foils were prepared from slices cut parallel to the basal plane, and also parallel to the $(01\bar{1}0)$ prism plane which contains the preferred shear direction $[\bar{2}110]$. In each instance, the foils were obtained from interior regions of the fatigued crystals. In contrast to bend fatigue damage, only minor variations in the dislocation substructure occur from region to region; FIGURE 4a may be considered representative of the dislocation structure existing on the basal plane after axial compression fatigue. Characteristic features include: three-fold nodes, angular dislocations by virtue of pinning effects, and a broad spectrum of dislocation loop shapes and sizes. Elongated loops have a direction of elongation along one of the three possible $\langle 10\bar{1}0\rangle$ directions in the basal plane.

The operative reflection ($g = 11\bar{2}0$) in FIGURE 4a gives rise to diffraction contrast for all dislocations having Burgers vectors of the form $\frac{1}{3}\langle 11\bar{2}0\rangle$. The dark field micrographs, FIGURES 4b and 4c, use two prism plane reflections. These produce conditions of zero contrast intensity for all line and loop dislocations having a Burgers vector in the reciprocal lattice plane normal to the respective prism plane directions. Therefore, line dislocations in the basal plane having a vector $\frac{1}{3}[11\bar{2}0]$ or $\frac{1}{3}[1\bar{2}10]$ can be made extinct using the $\bar{1}100$ and $10\bar{1}0$ reflections, respectively. Comparison of the bright field micrograph FIGURE 4 ($g = 11\bar{2}0$) with the pertinent dark field micrographs makes it clear that the line dislocations marked (A) become extinct using the $\bar{1}100$ reflection, FIGURE 4b. Dislocations marked (B) are extinct with the $10\bar{1}0$ reflection, FIGURE 4c. Since $\sum b = 0$,

and there are only two independent Burgers vectors in the basal plane, the leg (C) of the node ABC must be $\pm \frac{1}{3}[\bar{2}110]$. The elongated dislocation loop marked (1) is extinct only when the $10\bar{1}0$ reflection is operative; this is also the direction of elongation, suggesting that the Burgers vector is either $\frac{1}{3}[1\bar{2}10]$, or a lattice vector out of the basal plane but normal to this prism direction. In the former case, the loop would be an edge dipole. The small, nearly circular dislocation loops are extinct when using one of the three possible prism reflections. For example, the cluster marked (2) is extinct only when using the $\bar{1}100$ reflection. By a similar argument as that used for the elongated loop (1), the Burgers vector of these loops can be either $\frac{1}{3}[11\bar{2}0]$, or be out of the plane of the loop but still normal to the $[\bar{1}100]$ direction. It is certain that both the elongated and circular loops do not have a Burgers vector $\frac{1}{2}[0001]$, since they appear in strong contrast when using basal plane reflections.

In order to determine whether or not the loops are actually on the basal plane, slices were taken parallel to the prism plane containing the shear direction $[\bar{2}110]$. Therefore, the actual basal slip plane is viewed end-on, and any dislocation loops in this plane should appear as short single lines. The slices were taken from part of the same crystal as that represented by the micrographs in FIGURES 4a through 4c. A dark field micrograph of the prism plane slice where the $\bar{2}110$ reflection is responsible for contrast is included as FIGURE 4d. The bands of high dislocation density on the micrograph correspond to the basal plane trace. The large numbers of nearly circular dislocation loops seen clearly in the basal plane slices are now no longer resolvable, indicating that they do in fact lie on the basal plane.

b. Crystals Oriented for Prism Slip: The crystal oriented for bend fatigue on the $(0\bar{1}10)\ \frac{1}{3}[\bar{2}110]$ system was given 2×10^6 cycles at a resolved stress level on this system of 12,800 psi, and did not fracture. The slip structure and dislocation configurations were then examined on the tension surface. The fatigue damage on the surfaces subjected to maximum bending stress was characterized by the formation of a pronounced duplex slip structure, and by a distinct brownish discoloration, the intensity of which increased with increasing number of cycles (FIGURE 5a). The discoloration was confined to the two surfaces through which edge dislocations having the $\frac{1}{3}[\bar{2}110]$ Burgers vector emerge. The predominant bands are associated with the preferred prism slip system; however, examination of the surface reveals cross-slip on the basal plane where the resolved shear stress is very small. It is suggested that the discoloration is associated with the severe surface relief, and is a consequence of the repeated formation and rupture of an oxide film. In fact, repeated examination by polishing and replication has revealed the presence of persistent slip bands. These have been shown to be due to both intrusions and extrusions (12). The persistent slip structure remaining after the removal of an estimated 5μ from the surface is illustrated in FIGURE 5b. It is significant that no surface discoloration or persistent slip structure formed under conditions of bend fatigue when the slip was confined to the basal plane. In other words, cross-slip would appear to be important in the formation of the intrusions and extrusions, as has been deduced from other fatigue studies on close-packed crystal structures.

The transmission micrographs of foils prepared close to the tension surface show regions of high defect density which are not clearly resolved.

Presumably, these regions consist of glide dislocations and prismatic loops (FIGURE 6). During prolonged examination in the microscope, the defect structure underwent modification to one of clearly defined prismatic loops. The loops do not lie on the basal plane, which is normal to the foil, but appear to be on the active $(0\bar{1}10)$ prism plane. This apparent process of recovery is considered in more detail in the following section.

The axial tension fatigue specimens oriented for prism slip were given a total glide strain of 0.07. In this instance, the thin foils were prepared from slices cut parallel to the $(01\bar{1}0)$ prism plane, and also parallel to the basal plane which contains the $[\bar{2}110]$ shear direction. In contrast to the long straight prism slip bands seen after bend fatigue, the slip structure following fifty cycles of low frequency tension fatigue is characterized by relatively short prism slip traces, and connecting cross-slip traces on the basal plane (FIGURE 7a). The fine details of the intense prism slip bands are resolved by replication of this surface (FIGURE 7b). Damiano and Herman (5) have observed similar but less intense slip structures in identically oriented crystals after a comparable amount of unidirectional tensile shear strain.

FIGURE 8a illustrates the fatigue damage on the operative prism plane following axial tensile cycling. The substructure is in no way comparable to that observed on the operative basal plane following similar axial cycling (FIGURE 4a). However, the dislocation configurations on the basal plane of this specimen (FIGURE 8b) are similar to those on the basal plane illustrated in FIGURE 4a. The long lengths of the dislocations visible

in FIGURE 8b demonstrate clearly that slip has occurred on the basal plane; in this case this is the cross-slip plane which has a low resolved component of shear stress. None of the open dislocation loops seen on the basal plane slice can lie on any of the three possible prism planes. Many of the loops are elongated in the $[01\bar{1}0]$ direction which is normal to the operative Burgers vector, $\frac{1}{3}[\bar{2}110]$.

4. Recovery of Fatigue Damage

After prolonged examination of the bend fatigue crystal (basal slip orientation) in the electron microscope ($\sim$ 30 minutes), a most interesting sequence of events was observed which constitutes recovery in the transmission foil. The dislocation substructure of the fatigued state (FIGURE 3a) gave way to the sequence of configurations shown in FIGURE 9a through 9d. The line dislocations are seen to move over large distances on the basal plane (inclined at 43° to the plane of the foil), but the dislocation loops increase in size with only small lateral movement in the plane of the loop. Assuming that the loops are approximately circular, the projected shapes of the loops are compatible with their being on the basal slip plane. Consideration of FIGURE 9 shows that the loops marked 1 through 8 increase in size with increasing time of exposure in the electron microscope. Loops 1 and 2 eventually combine, and loops 3, 4, 6 and 8 have moved completely out of the foil. In this case, a 'ghost' image remains on the (0001) plane. Similar images remain as trails to the glide dislocations which have moved on the basal plane. In terms of the time scale, once the sequence of events had started, individual loops

changed size and moved out of the foil in a matter of seconds. A period $\sim$ 5 minutes was required to complete the recovery process such that the foil was completely devoid of glide dislocations and prismatic loops. The only way in which the loops can change size and position and give rise to the uniform 'ghost' image is by a combination of prismatic glide and climb. If climb were the only process, dislocation segments would remain in the foil anchored at the top and bottom surfaces, and, these would not give rise to complete 'ghost' loops.

A similar recovery process occurred in foils prepared from the bend fatigue crystal oriented for prism plane slip; the process involves similar times of exposure in the electron microscope followed by comparable rates of prismatic loop motion. In this case, the projected shapes of the dislocation loops were compatible with their being on the active $(0\bar{1}10)$ prism plane. It was not possible to promote recovery in the crystals subjected to axial fatigue deformation, even though the times and intensity of exposure in the electron microscope were increased. However, a foil from one of the axial compression fatigue crystals, oriented for basal slip, was set in a heating stage inside the electron microscope. In the temperature range 100-200^{o}C, rapid motion of glide dislocations was observed along with the annihilation or growth of prismatic loops. Above 200^{o}C the overall dislocation density became extremely low.

5. Discussion and Summary

In considering the dislocation substructure following bend and axial fatigue, it is important to be aware of any possible dislocation rearrangement processes. These may occur during the preparation of the foil,

or in the course of the observations in the electron microscope, as has been established for the bend fatigue foils. The extent to which the configurations are modified during thinning depends on the material. For aluminum, it is necessary to prepare foils $\gtrsim$ 2000Å in thickness in order to avoid rearrangement while the corresponding value in molybdenum is $\gtrsim$ 800Å. Experience with tapered foils of beryllium has shown that modification during thinning is restricted to areas of the foil below $\sim$ 700Å. A majority of the foils examined were in the thickness range 1000-2000Å and the dislocation configurations are considered to be representative of the bulk fatigued beryllium prior to any recovery processes. The stability of the substructure in the foil, within the microscope, is obviously related to the magnitude of the energy stored in the lattice by virtue of the fatigue damage. The bend fatigue mode gives rise to extremely localized deformation in the surface layers so that it is to be expected that recovery may be initiated by processes such as surface contamination in the microscope which gives rise to additional stresses in the foil. In comparison, axial fatigue gives rise to a uniform distribution of fatigue damage throughout the crystal. Recovery processes only occur if the foil is heated to temperatures $\gtrsim$ 100°C.

Axial fatigue for the basal slip orientation produces a uniform dislocation substructure with no apparent predominance of edge or screw component. This is in strong contrast to the substructure developed by unidirectional straining (Damiano and Herman 5) in crystals of identical orientation. In stage I of the tensile test long edge pairs and edge dipoles are present, suggesting that the screw are highly mobile on the basal plane. At higher strains (stage II), the presence of numerous edge

boundaries is associated with the onset of rapid work hardening. Differences also exist between the tensile and axial fatigue substructures in crystals oriented for prism slip. The tensile substructure, viewed on the prism plane, shows a predominance of screw dislocations (stage I); it is considered that the latter intersect the grown in networks and become jogged, thereby impeding motion. In stage II, complex interactions give rise to tangled masses of dislocations. The fatigue substructure observed on the prism plane is somewhat similar to that developed in stage II of the tensile test; however, this does not appear to be derived from a structure consisting initially of predominantly screw dislocations. Since the prism slip is accompanied by cross-slip on the basal plane, a tangled dislocation configuration is to be expected if no recovery processes take place.

Unfortunately, it has not been possible to determine the Burgers vector of the prismatic dislocation loops. The diffraction contrast experiments have established that the vector is out of the plane of the loop but is not perpendicular to the plane of the loop. Since the larger loops do not show stacking fault fringes, it is tempting to assume that they have a perfect lattice vector; however, it must be remembered that the appropriate extinction distances in beryllium are large and actually approach the foil thickness ($\sim$ 1500Å). It is therefore possible that stacking faults are present but are not visible under the diffraction contrast conditions. Further observations are being made on these loops in an attempt to clarify the situation. With a knowledge of the loop vector it is then possible to consider the details of the recovery process.

Acknowledgments

The authors wish to thank Mr. Wayne D. Hepfer for assistance in preparation of the transmission foils and surface replicas.

References

1. Wallace, W. P., and Wallace, R. M., Light Metal Age, Vol. 13, 19 (1955).

2. Klein, J. G., Perelman, L. M., and Bever, W. W., Brush Beryllium Co. Rep. No. WADS-TR58478 (Part 1), (1958).

3. Wilhelm, F., and Wilsdorf, H. G. F., Franklin Institute Report on Air Force Contract No. AF 33(616)-7065, March 1963.

4. Walters, G. P., van der Walt, C. M., and Makin, M. J., Conference on Physical Metallurgy ofBeryllium, USAEC, Gatlinburg, Tennessee, May 1963.

5. Damiano, V. V., and Herman, M., Materials Science Research, Vol. II, Plenum Press, New York 1964.

6. Segall, R. L., Electron Microscopy and Strength of Crystals, p. 515 Interscience, New York 1963.

7. Berghezan, A., Fordeux, A., and Amelinckx, S., Acta Met. 9, 464 (1961).

8. Segall, R. L., Partridge, P. G., and Hirsch, P. B., Phil. Mag., 6, 1493, (1961).

9. Spangler, G. E., Herman, M. and Ardnt, E. J., Dept. of Navy, Bureau of Naval Weapons, Contract No. W61-0221-d (1961).

10. Breedis, J. F., Lawley, A., and Zeiger, J., NASA Contract No. NASr-145, April (1964).

11. Grube, W. L., and Rouze, S. R., Proc. ASTM, 52, 573 (1952).

12. Breedis, J. F., and Lawley, A., to be published.

TABLE 1

Crystallographic Code for Fatigue Crystals

Fatigue Mode	Plane Code (A)	Plane Code (B)	ϕ	Favored Slip System
Reverse Bend	$(0\bar{1}10)$	(0001)	43°	(0001) 1/3 $[\bar{2}110]$
Simple Bend	(0001)	$(0\bar{1}10)$	48°	$(0\bar{1}10)$ 1/3 $[\bar{2}110]$
Cyclic Compression	$(0\bar{1}10)$	(0001)	80°	(0001) 1/3 $[\bar{2}110]$
Cyclic Tension	(0001)	$(0\bar{1}10)$	48°	$(0\bar{1}10)$ 1/3 $[\bar{2}110]$

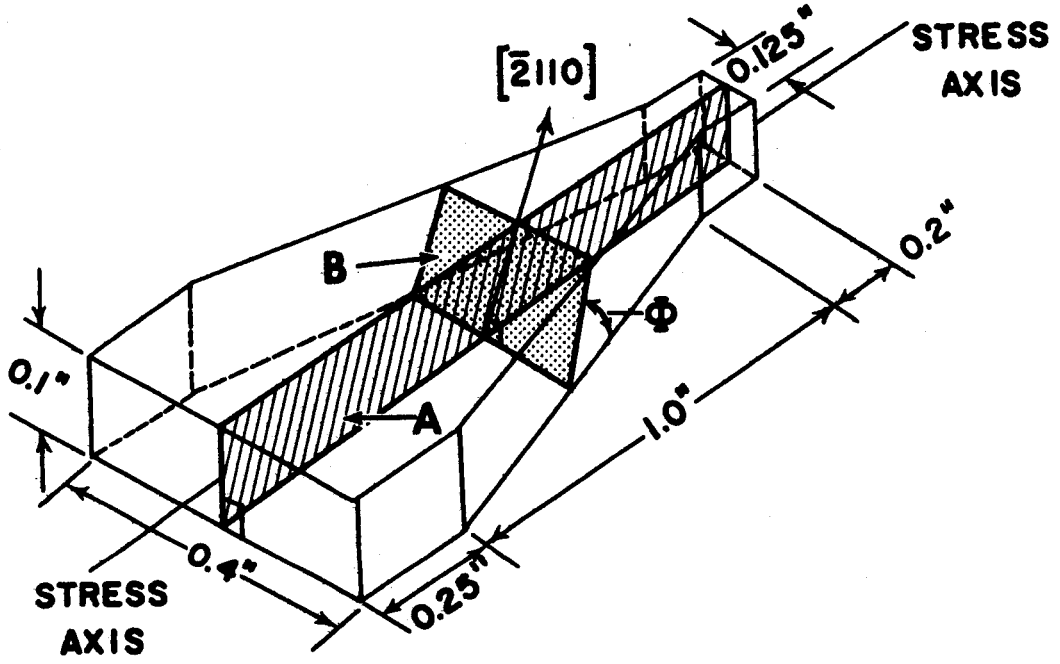

(a)

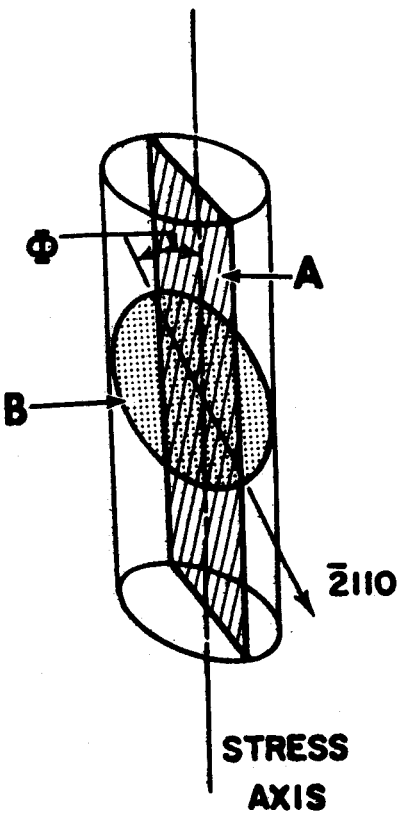

(b)

FIGURE 1

The geometry and dimensions of the beryllium single crystal specimens (a) bend fatigue (b) compression fatigue (c) tensile fatigue

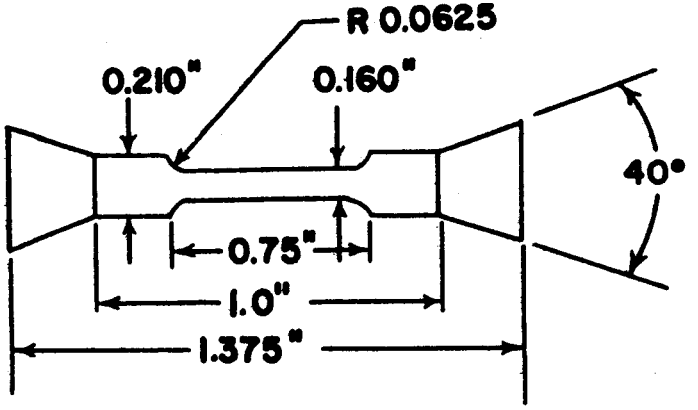

(c)

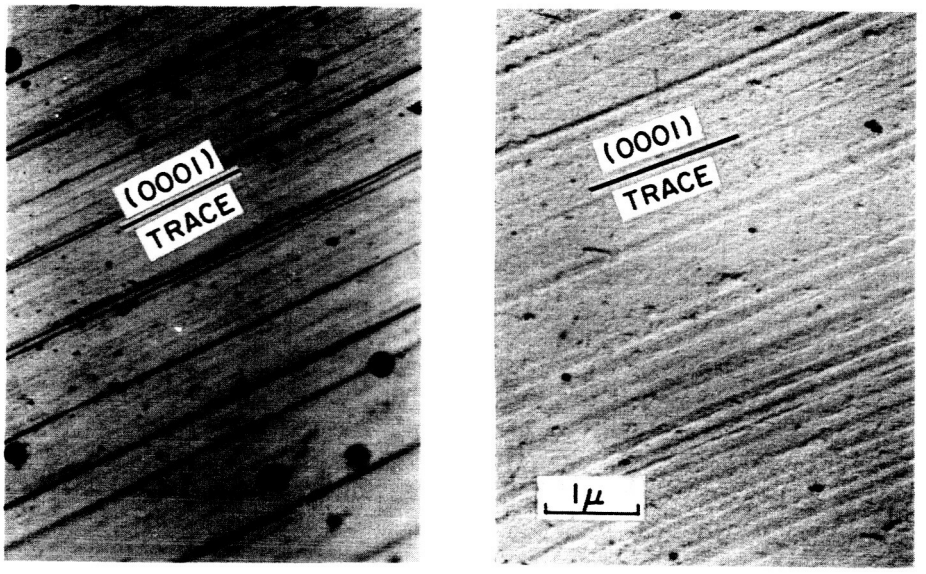

(a) (b)

FIGURE 2

(a) Optical Micrograph of the slip band structure at the surface of the bend fatigue crystal near the grip. Basal slip orientation X 200. (b) Surface replica from region close to grip.

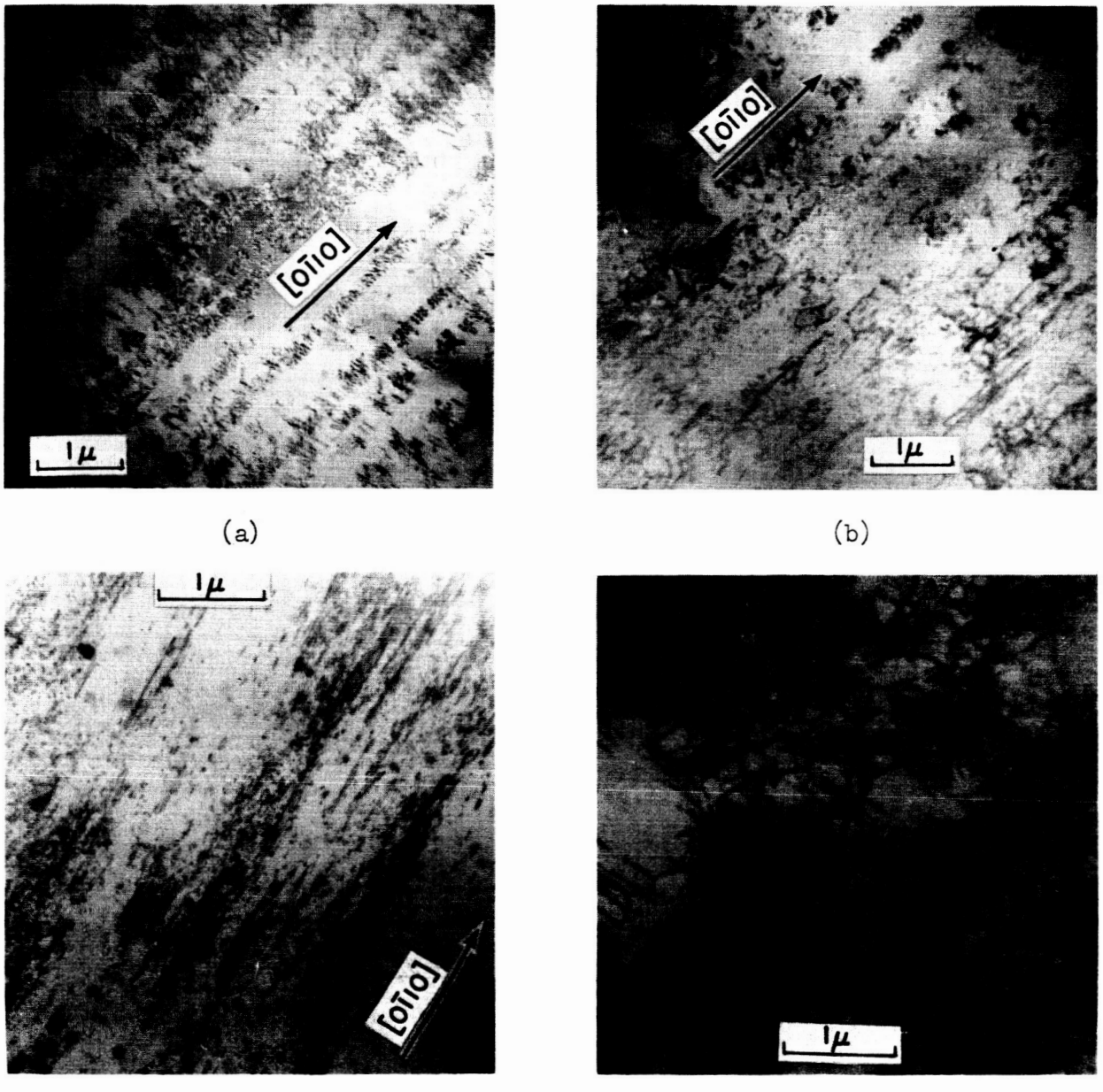

FIGURE 3

Dislocation substructure close to the bend surface in a crystal oriented for basal slip in bend fatigue. Plane of foil is $(\bar{2}113)$.

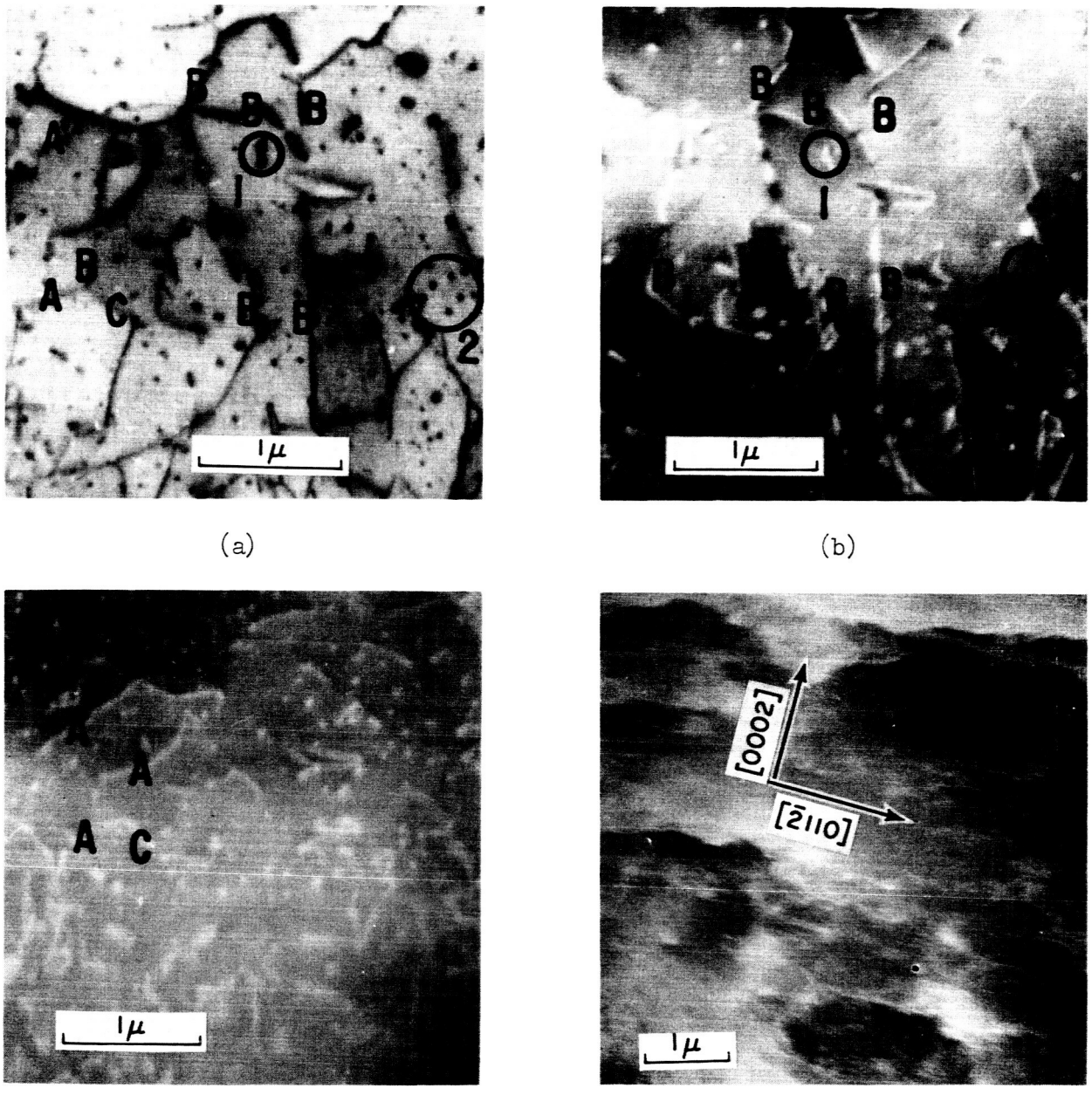

FIGURE 4

Light and dark field micrographs of the dislocation substructure following axial compression fatigue. Crystal oriented for basal slip. Foil plane is (0001) in a, b, c and $(01\bar{1}0)$ in d. Operative reflections are: $11\bar{2}0$, $\bar{1}100$, $10\bar{1}0$, $\bar{2}110$, in a, b, c, d respectively.

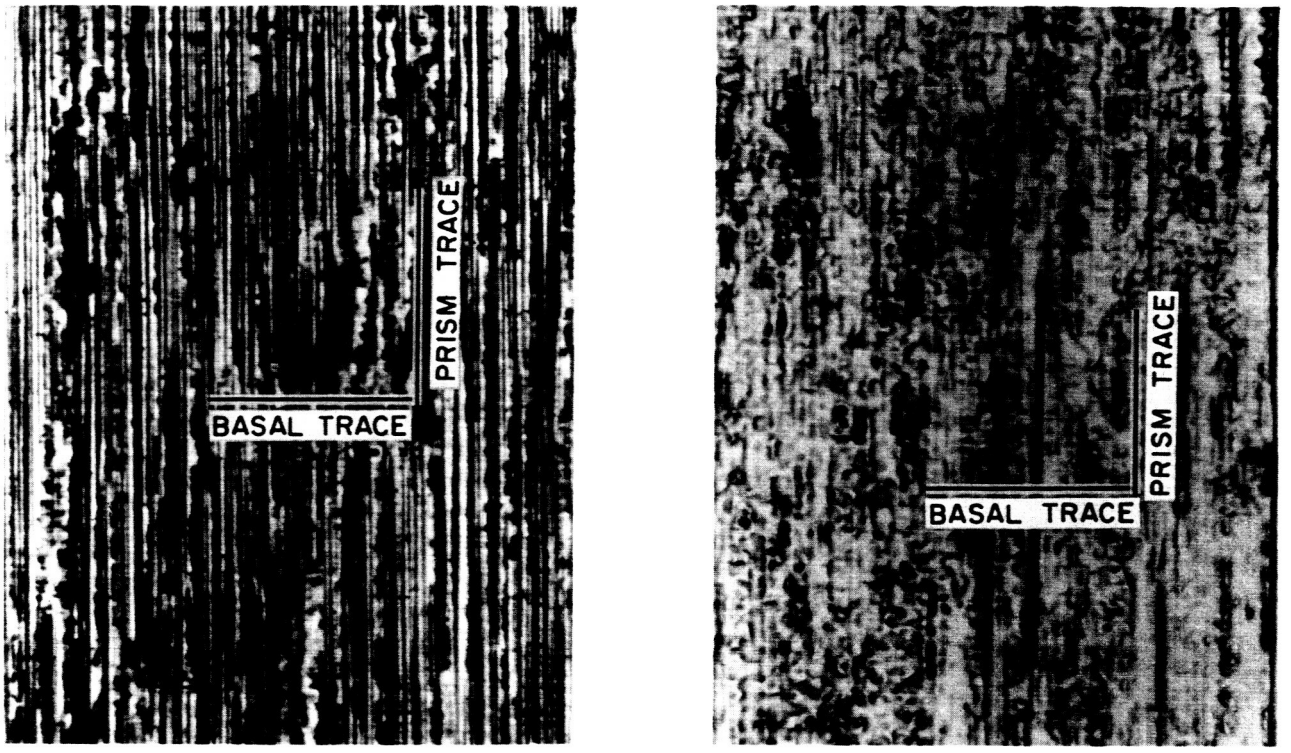

(a) (b)

FIGURE 5

Optical micrographs of the slip band structure at the surface of the bend fatigue crystal oriented for prism slip (a) as fatigued (b) fatigued and electropolished to a depth $\sim 5\mu$. X 300.

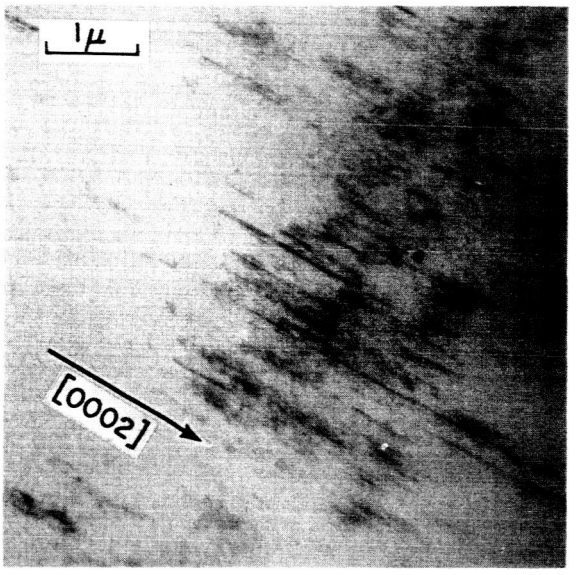

FIGURE 6

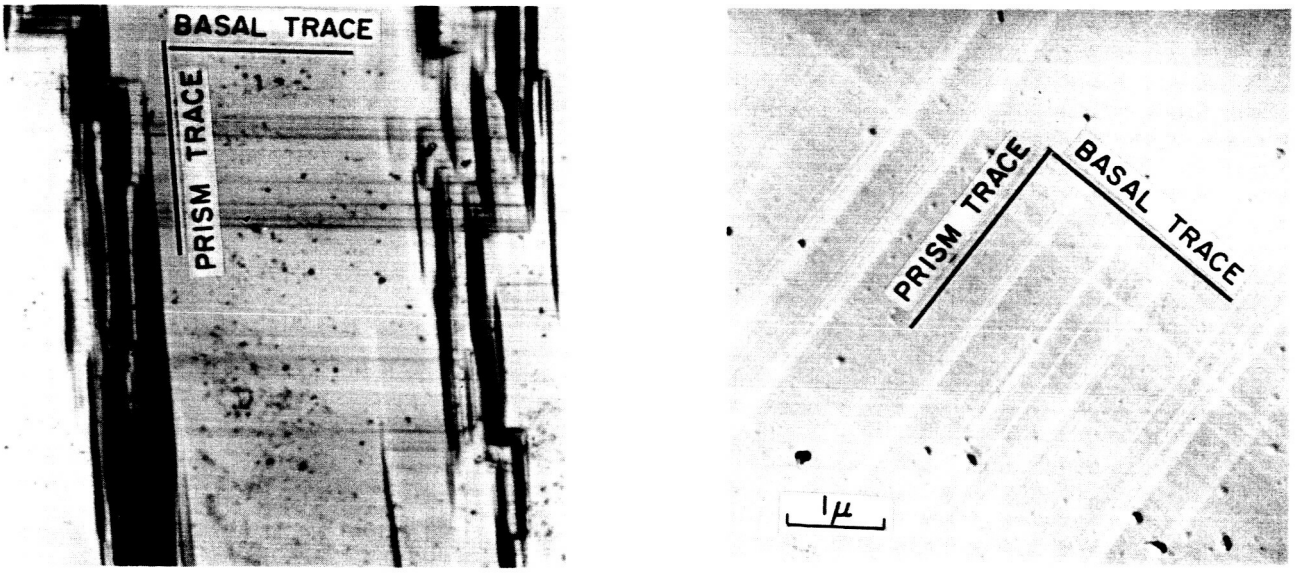

(a) (b)

FIGURE 7

(a) Optical micrograph showing prism and basal plane slip. Axial tensile fatigue in crystal oriented for prism slip. X 300. (b) Corresponding slip structure by surface replication.

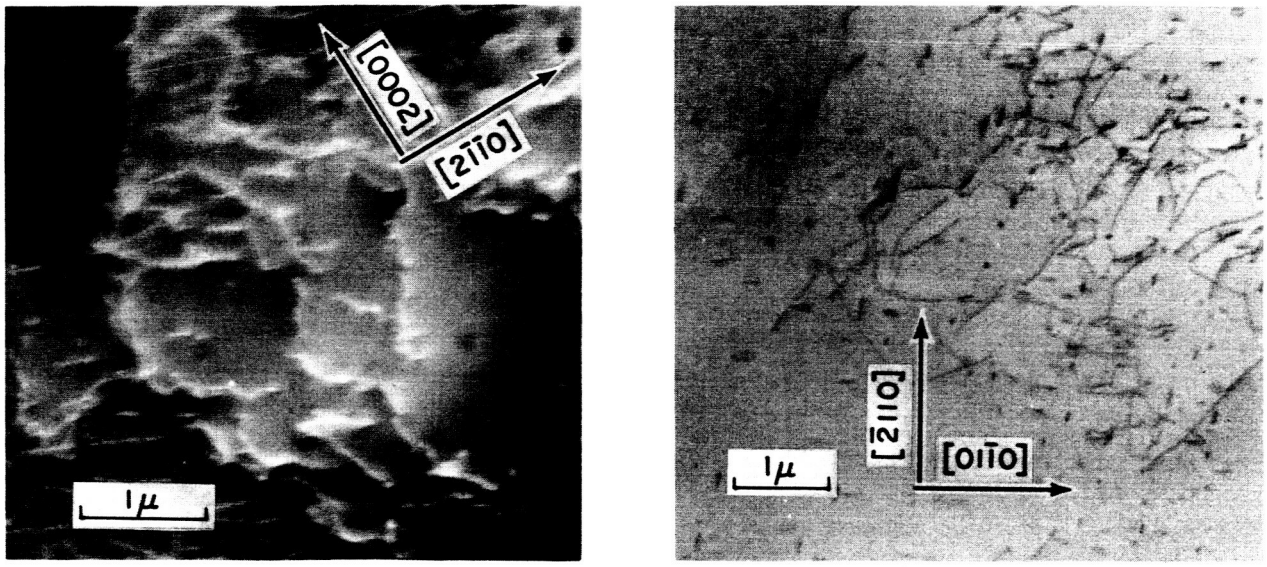

(a) (b)

FIGURE 8

Dislocation substructure following axial tensile fatigue in crystal oriented for prism slip. (a) plane of foil (0$\bar{1}$10), operative reflection $\bar{2}$110. (b) plane of foil 0001.

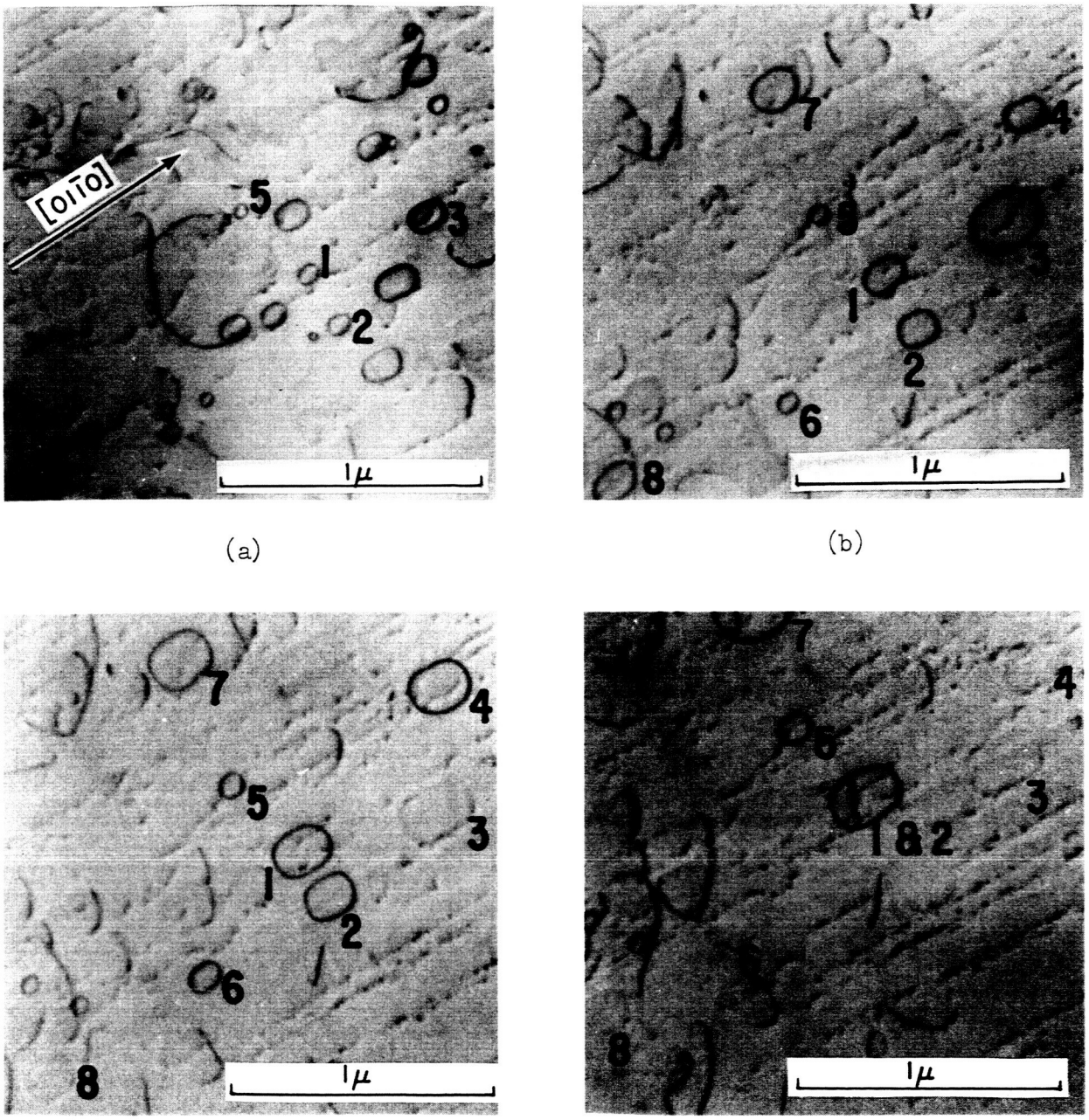

FIGURE 9

Sequence of recovery events in crystal originally deformed in bend fatigue. Basal slip orientation. Plane of foil ($\bar{2}113$).